Appl Phys A (2011) 105:881–890
DOI 10.1007/s00339-011-6518-6

Applied Physics A
Materials Science & Processing

Aqueous chemical growth of free standing vertical ZnO nanoprisms, nanorods and nanodiskettes with improved texture co-efficient and tunable size uniformity

S.D. Gopal Ram · G. Ravi · A. Athimoolam · T. Mahalingam · M. Anbu Kulandainathan

Received: 19 June 2011 / Accepted: 21 June 2011 / Published online: 29 July 2011

Abstract Tuning the morphology, size and aspect ratio of free standing ZnO nanostructured arrays by a simple hydrothermal method is reported. Pre-coated ZnO seed layers of two different thicknesses (≈350 nm or 550 nm) were used as substrates to grow ZnO nanostructures for the study. Various parameters such as chemical ambience, pH of the solution, strength of the Zn^{2+} atoms and thickness of seed bed are varied to analyze their effects on the resultant ZnO nanostructures. Vertically oriented hexagonal nanorods, multi-angular nanorods, hexagonal diskette and popcorn-like nanostructures are obtained by altering the experimental parameters. All the produced nanostructures were analysed by X-ray powder diffraction analysis and found to be grown in the (002) orientation of wurtzite ZnO. The texture co-efficient of ZnO layer was improved by combining a thick seed layer with higher cationic strength. Surface morphological studies reveal various nanostructures such as nanorods, diskettes and popcorn-like structures based on various preparation conditions. The optical property of the closest packed nanorods array was recorded by UV-VIS spectrometry, and the band gap value simulated from the results reflect the near characteristic band gap of ZnO. The surface roughness profile taken from the Atomic Force Microscopy reveals a roughness of less than 320 nm.

S.D.G. Ram
Department of Physics, Bharath Niketan Engineering College, Aundipatti 625 536, India

G. Ravi (✉) · T. Mahalingam
Department of Physics, Alagappa University, Karaikudi 630 003, India
e-mail: gravicrc@gmail.com
Fax: +91-04565-225202

A. Athimoolam
Department of Physics, Fatima Michael College of Engineering and Technology, Madurai 625 020, India

M.A. Kulandainathan
Central Electro Chemical Research Institute, Karaikudi 630 006, India

1 Introduction

The demand for new, cost effective methods and processes for the preparation of controlled and extended growth of nanostructures of various materials are continuously on the increase, since the dimensions of a variety of devices based on nanostructures are ever decreasing [1–3]. Among the materials, zinc oxide (ZnO) is a promising and a versatile candidate since it possesses suitable properties such as a wide band gap (3.37 eV) and a large exciton binding energy of 60 meV [4–6]. ZnO vertically aligned nanowire arrays draw more interest among the researchers around the globe for their attractive applications in nanoscale transistors, electronic-nose, light emitting devices, and field emission devices [7–9]. For the preparation of ZnO nanostructures, the hydrothermal method is one of the best methods in industrial applications, since this method has the advantages such as rapid and a low-cost technique compared to vapour phase methods. This is evident from the recent reports on the synthesis of ZnO nanostructures in different temperature and time durations [10–12].

Herein, we present the inferences of the investigations on the hydrothermal growth of ZnO nanostructures on chemical bath deposited ZnO seed layers. The seed layers are more coveted as they provide an epitaxial effect on the crystalline orientation of nanorods. The seed can offer an electron matching between the empty dangling bonds of the surface zinc atoms and filled dangling bonds of surface oxygen

Table 1 Experimental parameters implemented for preparing various ZnO nanostructures

Serial No.	Sample ID	Reaction media	Seed layer thickness	pH
1	ZnO-A	0.03 M—$ZnSO_4 + NH_3$	Single (350 nm)	12
2	ZnO-B	0.03 M—$ZnSO_4 + NH_3$	Double (550 nm)	12
3	ZnO-C	0.02 M—$ZnSO_4 + NH_3$	Single	12
4	ZnO-D	0.02 M—$ZnSO_4 + NH_3$	Double	12
5	ZnO-E	0.03 M—$ZnSO_4$ + HMT + NaOH	Double	12
6	ZnO-F	0.03 M—$ZnNO_3$ + HMT	Double	6–7
7	ZnO-G	0.03 M [$ZnNO_3 + Zn(Ac)_2$] + HMT	Double	6–7

atoms with compensation of the internal dipolar moment of the wurtzite structure [13]. Therefore, advantages of the seed layer are constructively exploited as a platform for tuning the size and shape of the ZnO nanostructure. The possibilities of producing tailor-made nanostructures by altering the experimental conditions like the thickness of the seed layer, source of zinc cations, and hydroxyl anion producing agents are considered and experimented. The obtained nanostructures are observed and the possible differences in growth kinetics due to the chemical routes for the production of these nanostructures are elucidated.

2 Experimental methods

Aqueous chemical growth of ZnO nanostructures was carried out by using different Zn salts such as $Zn(NO_3)_2{\cdot}6H_2O$, $ZnSO_4{\cdot}7H_2O$, Zn $(CH_3COO)_2{\cdot}2H_2O$. Suitable mineralisers like ammonia, hexamethylenetetramine (hexamine), and NaOH, were used after several trial and error experiments. In a typical experiment (ZnO-A to D), the reactant precursor was prepared by mixing 0.03 M of zinc sulphate heptahydrate ($ZnSO_4{\cdot}7H_2O$), and 5 ml of 25% ammonia solution with 75 ml of distilled water. The aqueous mixture was stirred for 15 minutes at room temperature to obtain a homogeneous white solution. The precursor solution becomes milky at first and then turned clear quickly due to the formation of the zinc–amine complex. The pH of the solution was noted, and then the solution was transferred into 100 ml autoclavable borosilicate glass bottles at a filling ratio of 80%. A seed layer, already prepared by successive immersion of chemical-etched corning micro-slide alternatively in ammonium zincate at the ambient temperature and a hot water bath kept at near boiling temperature (∼95°C) and was subsequently dried in hot air [14, 15]. This pre-coated glass substrate with an adherent zinc oxide layer was immersed into the precursor solution in order to provide a uniform platform for easy nucleation, uniform coverage over the substrate, improved texture, and enhanced growth along the substrate. Further, the reaction vessel was sealed by a polypropylene screw cap to render the vessel free from any leakage in such a way to withstand the pressure developed during the hydrothermal process [16]. After the solution mixture was pretreated under the laboratory oven, the reaction temperature was quickly increased to 115°C and maintained at the same temperature for 5 hours before the reaction was terminated. The autoclave was cooled to room temperature by natural means and the same procedure was followed for the preparation of all the other samples. In some cases, the thickness of the seed layer was increased to two-fold. The thickness of the seed layer can be linearly increased with the number of dippings or increasing the zinc concentration [14]. Three different sets of Zn metal salt combinations, two sets of seed layer thicknesses, and two different concentrations of same Zn metal salts are experimented. Various modified experimental parameters applied for the preparation of differently shaped vertically aligned free standing ZnO nanorods are tabulated in Table 1.

3 Characterisation

The crystalline structures of the as-prepared films were analysed by PANalytical X'pert PRO X-ray diffractometer, Scanning Electron Microscopy (SEM) analysis was taken using the Hitachi Model S-3000 H instrument, for their structural and morphological properties respectively. The XPS measurement was taken by VG electron Spectroscope within the scanning binding energy range 0–1200 eV to confirm the obtained mineral layer was pure ZnO. The surface smoothness of the prepared nanostructures are observed by Atomic Force Microscopy (AFM). The size distributions of three nanostructures of ZnO are given by a histogram to compare the variation in aspect ratio.

4 Results and discussion

4.1 X-ray diffraction analysis

From the XRD patterns (Fig. 1) observed for six different ZnO nanostructures, it can be inferred that the experimental conditions influence the crystallinity of the nanostructures.

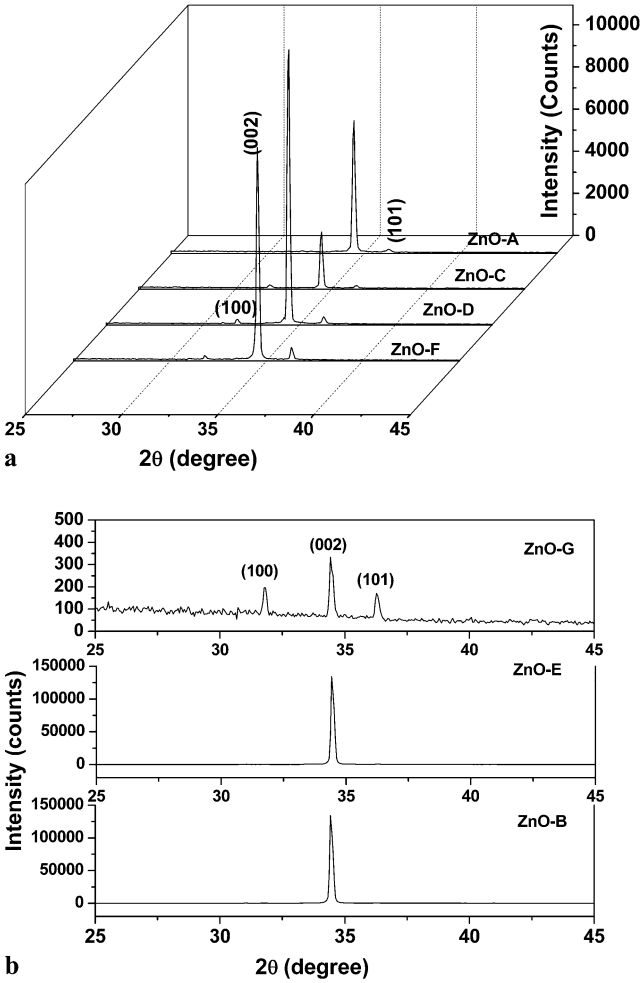

Fig. 1 (**a**) X-ray diffraction patterns of ZnO nanostructures having intensity in the region of 2500 to 8500 counts (**b**) ZnO-B & E showing a very high intensity, and ZnO-G (the diskette-like structure) showing a very low intensity than other structures

This is evident from the intensity variations observed in the X-ray diffraction patterns. For the experimental combinations of ZnO-B and ZnO-E, the intensity of the X-ray reflections is up to 140,000 which is the highest of any other structure (Fig. 1b). In both the cases (ZnO-B, ZnO-E), a double thick seed layer was used.

The double thick seed layer has produced a vast difference in the intensity of the preferred orientation peak. This illustrates that the thicker seed layer has an effect on the growing nanocrystals. When the zinc metal ion concentration is higher, then it has also favoured a stronger peak in the preferred orientation, or in other words improved crystallinity along the growth axis. This is inferred from the peak intensities of the X-ray diffractograms. Among the nanostructures ZnO-B and ZnO-D, the intensity of ZnO-B, which is prepared from the 0.03 M $ZnSO_4$ precursor solution, is higher. The thicker seed layer may have an enhancing effect on heterogeneous nucleations and the higher molar strength

Table 2 Lattice parameter, cell volume, Texture co-efficient values of different ZnO nanostructures—derived from the X-ray diffraction data

Sample ID	Lattice constant (Å)		c/a ratio	Cell volume (Å^3)	Texture coefficient
	'a'	'b'			
ZnO-A	3.212	5.203	1.6	47.631	2.243
ZnO-B	3.326	5.264	1.582	50.456	3.504
ZnO-C	3.249	5.202	1.601	47.579	2.827
ZnO-D	3.250	5.204	1.601	47.601	3.489
ZnO-E	3.232	5.220	1.615	47.229	3.495
ZnO-F	3.248	5.194	1.599	47.46	3.490
ZnO-G	3.248	5.203	1.602	47.544	1.891
Standard value	3.249	5.206	1.633	46.802	–

can support a stronger supersaturation. But, on the contrary, when the X-ray diffraction patterns show sharp crystalline peaks, their lattice parameters calculated exhibited a deviation from the standard cell parameters as shown in Table 2. The table gives the details of the lattice constants 'a', 'c', the cell volume, and texture coefficients of the samples. All the above parameters were calculated using the 'd' spacings of the dominant peak in the XRD pattern of the corresponding nanostructure. The texture coefficient was calculated from the formula, previously reported by Mahalingam et al. [17].

5 XPS analysis

For the identification of ZnO by its binding energy in XPS spectra, C 1s at 286.4 eV was used. The recorded XPS spectrum is shown in Fig. 2(a)–(c). The binding energy spectra of Zn $2p_{3/2}$ and Zn $2p_{1/2}$ are 1022.9 eV and 1045.95 eV, respectively. At 531.5 eV, the O 1s peak is found. The above results confirm the standard binding energy of the ZnO [18].

6 Morphological analysis

The Scanning Electron Microscope images show a variety of shapes of zinc oxide nanostructures such as vertical hexagonal nanorods (Fig. 3a,b), skewed nanorods (Fig. 3c,d) bunches of pencil-like tipped nanorods (Fig. 3e,f), uniformly sized nanotwigs (Fig. 3g,h), very closely packed nanofibres (Fig. 4a,b), hexagonal diskette-like structure (Fig. 4c), popcorn-like concave finished particles (Fig. 4d,e) which are produced from various experiments numbered viz. ZnO-A to ZnO-G, respectively. These variations are caused by the difference in the chemical ambience and subsequently due to various growth kinetics.

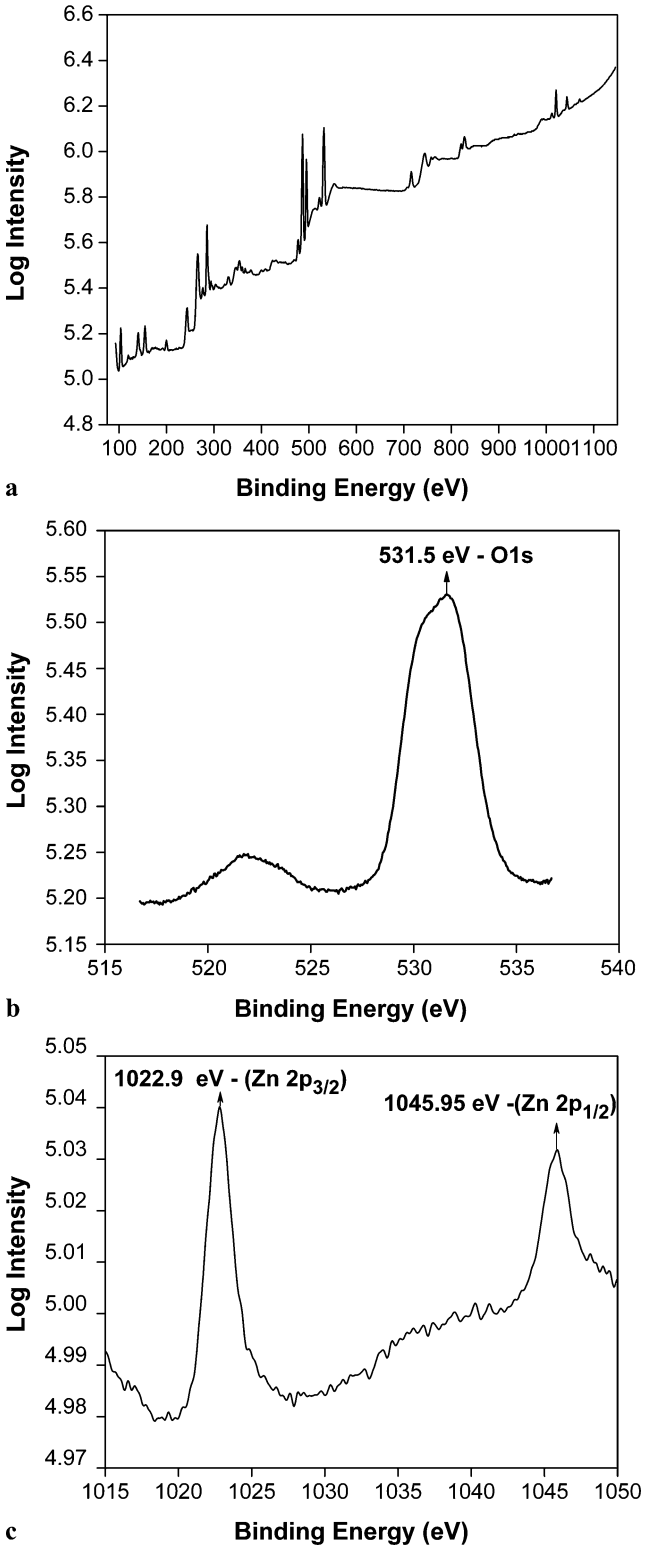

Fig. 2 XPS spectra of ZnO nanorods array: (**a**) full scale survey spectrum of sample, (**b**) O 1s spectrum, (**c**) Zn 2p spectrum

As seen from Table 2, particularly ZnO nanostructures synthesised from the higher $ZnSO_4$ concentration with thicker seed layer shows more deviations from the standard cell parameters whereas the rest of the nanostructures are showing near standard values. But sample ZnO-B exhibited the highest texture co-efficient. Therefore, due to faster growth, this particular nanostructure might have incorporated more defects such as oxygen vacancies or Zn interstitials.

In the case of ZnO-A, closely packed hexagonal ZnO nanorods vertically aligned onto the substrate are formed. They are synthesised from 0.03 M of zinc sulphate solution added with a suitable amount of NH_3, on a seed layer coating of single layer thickness. Here, most of the nanorods have the diameter of nearly 100 nm. Their shape is a bit uneven, but the structures are closely packed. When a layer with double thickness was used as a seed for the growth (ZnO-B), well-defined hexagonal nanorods, having different diameters ranges have emerged and most of them are crisscrossing each other or skew in nature. But, they are all free standing from the seed layer which are shown in Fig. 3(c,d). On the doubly thick seed layer, the hexagonal solid rod-like structures seem to exhibit an enhanced growth, and this can be attributed to the increase in the seed-bed depth alone that has supported the nanostructures a free standing growth. This is more advantageous in growing nanostructures of high aspect ratio which are the most desirable for the fabrication of devices.

By reducing the Zn metal ion concentration in the solution (0.02 M $ZnSO_4$), a bunch of nanorods with peculiar pencil-like tips (ZnO-C) are formed on the single layer seed. This can be attributed to the faster growth velocity along the (0001) phase. The growth velocities of different growth phases are as follows [19].

For, $V_{(0001)} > V_{(\bar{1}0\bar{1}1)} > V_{(\bar{1}010)} > V_{(101\bar{1})} > V_{(000\bar{1})}$, the same precursor concentration (0.02 M), when grown on double layer thick seed, skewed nanotwigs of uniform dimension (ZnO-D) is formed. Here, the depth of the seed layer provides the platform for uniform and easy heterogeneous nucleation [20]. So, it is identified that the aspect ratios of the produced morphologies can be tuned by altering the ionic strength and nucleation kinetics by providing a seed layer in the solution.

Adding NaOH and hexamine as anion generating sources, a good texture and a closest packing of nanofibres array is obtained (ZnO-E). These kinds of size uniformity and full coverage is highly preferable. The solution made from zinc nitrate hexahydrate and hexamine, has produced a hexagonal diskette like morphology (ZnO-F) with a suppressed axial growth. In this chemical ambience, the radial growth has dominated the axial growth. Here also, the double layer thick seed was used. In the precursor of the aforesaid experiment, when zinc acetate dihydrate was also added, they

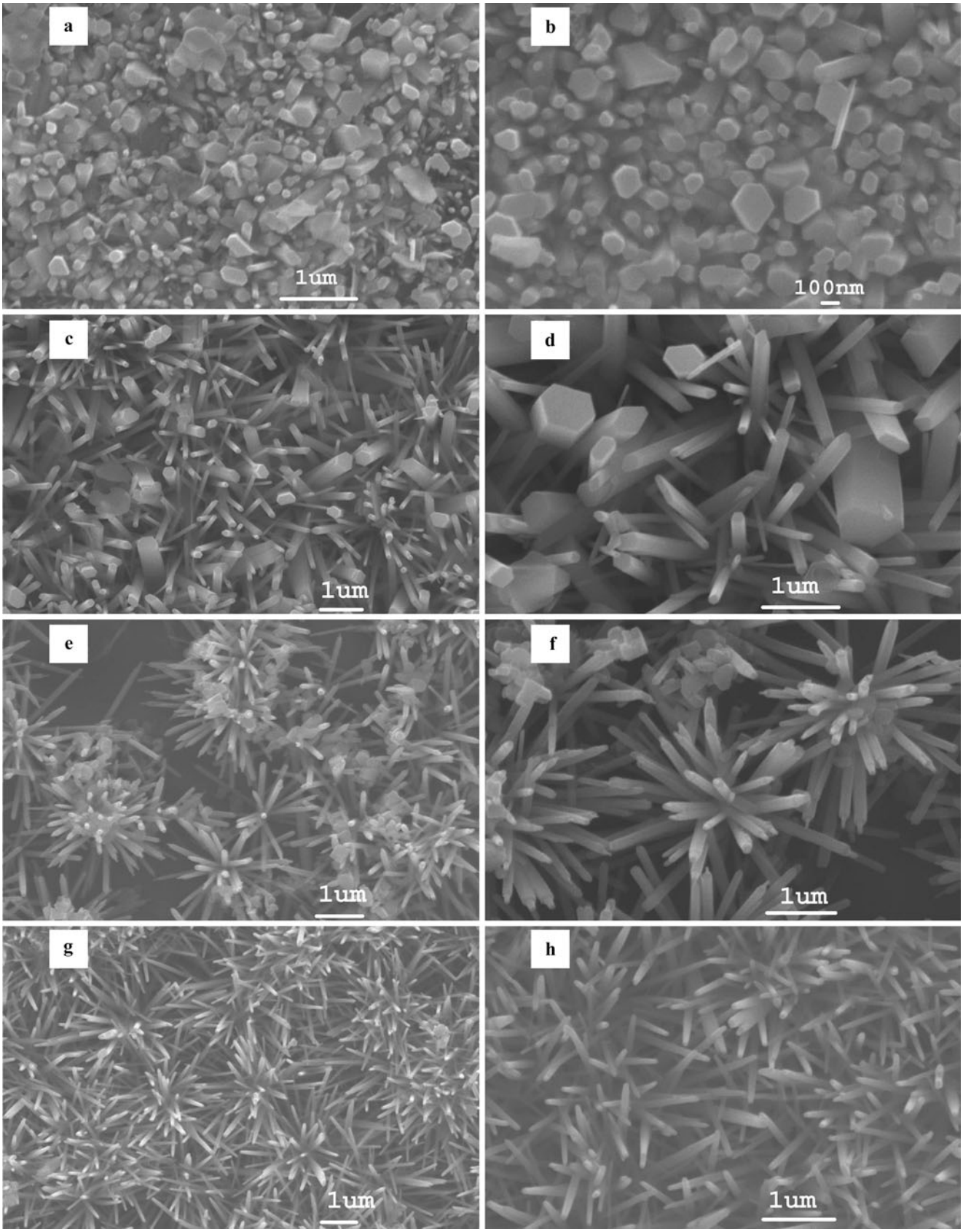

Fig. 3 Scanning Electron Microscopy images of ZnO nanostructures: (**a**), (**b**) morphology of ZnO-A, prepared from 0.03 M $ZnSO_4$ using single layer seed; (**c**), (**d**) 0.03 M $ZnSO_4$ on double layer seed; (**e**), (**f**) 0.02 M $ZnSO_4$ on single layer seed; (**g**), (**h**) 0.02 M $ZnSO_4$ on double layer seed

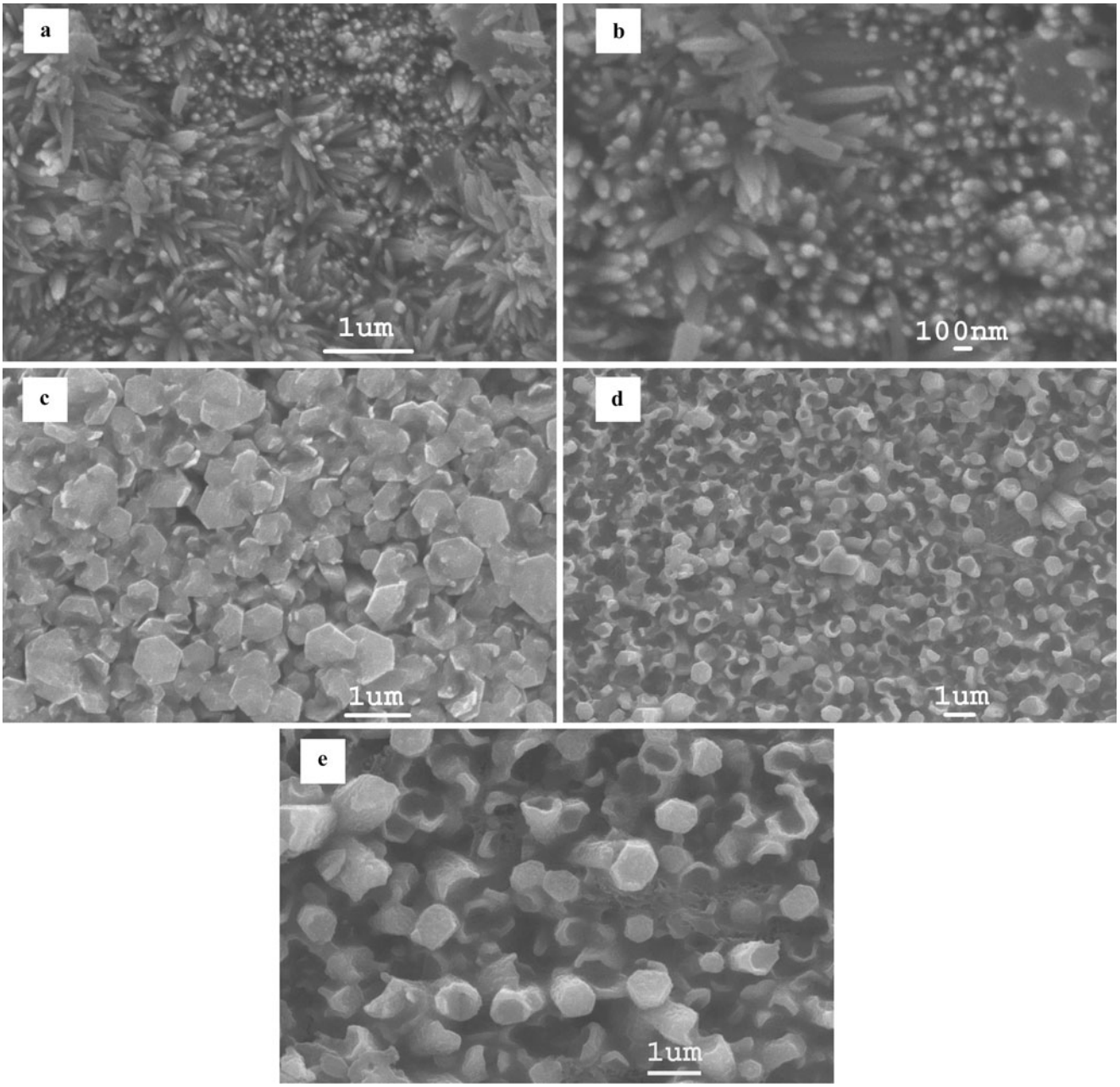

Fig. 4 SEM images (**a**), (**b**) the closest packed ZnO nanostructure produced with the aid of HMT and NaOH; (**c**) Hexagonal diskettes resulted from HMT and $ZnNO_3$; (**d**), (**e**) Popcorn like nano-ZnO obtained from mixture of $ZnNO_3$, $Zn(Ac)_2$ and hexamine

have favoured the formation of peculiar popcorn like external finishing with a cavity (ZnO-G). But when zinc acetate alone was used as the Zn ion source, they did not yield good results, with ammonia and (HMT + NaOH) in separate reactions. The concave finishing of the structures may be due to a reverse dissolution process. As the growing structures attract the ZnO precursors from the mother liquor with a faster rate, at a particular stage of growth, the mother liquor would have supplied more than what it can actually supply losing an electrostatic equilibrium, in other words gets under saturated. Hence, the system turns unstable. In unstable conditions, Ostwald's ripening is more pronounced. So, the coarsening, i.e., the growth of bigger particles at the cost of the smaller ones takes place. In addition, the system will try to come back to the equilibrium retaining a minimum amount of Zn^{2+} ions in the solution. Hence, the dissolution of the grown nanostructures takes place. As a result, the top most layer gets dissolved which causes the grown nanostructures to get a concave finishing at the grown end. This could be a viable reason for the concave

or porous feature of the ZnO nanostructures in ZnO-G sample.

The histograms constructed from the SEM images of ZnO-A, ZnO-B and ZnO-F are seen in Fig. 5(a–c). The histogram in Fig. 5(a), shows that there are maximum number (nearly 45% of the total population) of hexagonal nanorods formed in the diameter range of near about 100–125 nm. In the rest, 30% of the hexagonal prisms are having diameters even less than 100 nm. Figure 5(b), represents that 60% of the occurrences are in the diameter region of less than 175 nm in the total population. From these two representations, it is obvious that the increase in the seed layer has clearly influenced the diameter of the nanorods. In the latter case, the maximum number of nanostructures are in the diameter scale of 250 nm, where as it was nearly 110 nm when the seed bed had a single layer thickness. In Fig. 5(c), the histogram representation of the nanodiskette-like structure is given. The picture depicts that the maximum number of the diskettes lie in the cross section length of 350 nm. But still, their aspect ratio was appreciable, as they had a suppressed growth along the axial direction giving a more surface area, which is preferable.

As explained earlier, using the seed layer has advantages as it promotes easier nucleation and subsequent growth by rendering an epitaxial effect on the crystalline orientation for the further growth of nanostructures by the way of providing electron matching between empty dangling bonds (zinc and oxygen) on the surface and the growth units in the solution. Parallel and perpendicular orientation of the nanostructures can be tuned by limiting the nucleations [16]. Homogeneous nucleations from solutions require higher activation energy barrier, and eventually, they are less favourable and heterogeneous nucleations spontaneously take over. Therefore, a seed layer can favour heterogeneous nucleations on the substrate, and homogeneous nucleations occur in the bulk solution [20]. In the double thick layer, there is more possibility of nucleations arbitrarily on any location of the seed layer due to the electrostatic affinity and easy attachment of the freshly produced Zn^{2+}, hydroxyl (OH^-) ion complexes to the existing epitaxial layer. But, in this case, the ionic strength of the solution is changed. When the ionic strength is higher (0.03 M), the nanostructures produced are of perpendicular orientation. On the contrary, for 0.02 M, a multiangular orientation with a sea urchin- like morphology has resulted.

The skew nature or tilted orientation of the grown ZnO nanorods is detected as a common feature among ZnO nanorods. They exhibit an angle of inclination of 52° to the z-axis, perpendicular to the plane of the substrate [21]. The structure ZnO-C exhibits peculiar pencil tip like structure which is absent in this case, when double layer seed was used. In either of the cases, the ionic strength is the same and eventually the probable population of metal cations will

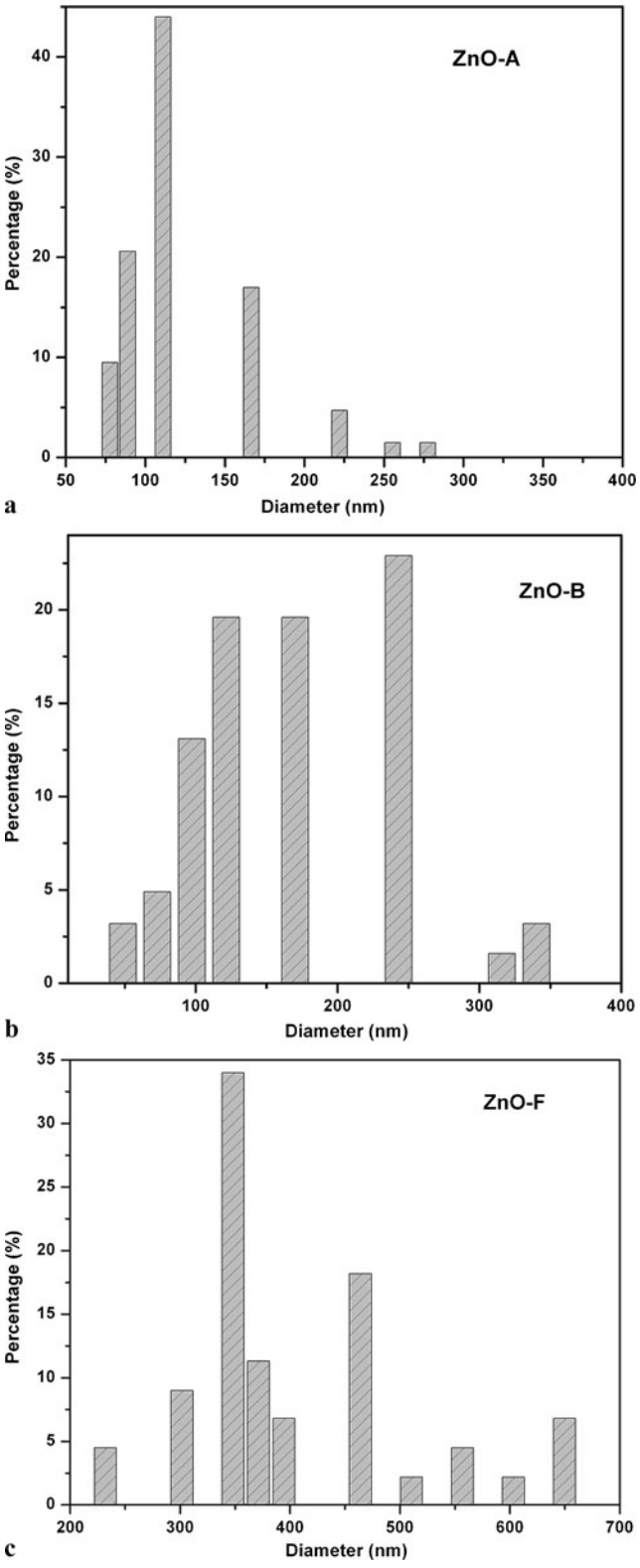

Fig. 5 Histograms depicting the diameter variations and percentage of particles in a particular diameter in the three different nanostructures of ZnO (**a**) ZnO-A, (**b**) ZnO-B and (**c**) ZnO-F

follow. But, in the former case, it is suspected that some of the produced metal cations could have been consumed for the production of nucleation units. In the latter case (ZnO-D), this may be lesser, since a large numbers of metal cations are not consumed for the nucleation in the pre-existing double layer.

By increasing the ionic strength of a medium, the interfacial energy can be reduced [16]. Therefore, when the precursor concentration increases, the nucleation of zinc oxide is rapid, and more ZnO nuclei form in the initial stage. These nuclei may aggregate together due to excess saturation. Each of them individually grows along the c-axis into rod like crystal, and thus the formation of urchin-like architectures are obtained.

7 Growth kinetics

In the hydrothermal process, the growth unit of ZnO is $[Zn(OH)_4]^{2-}$, leads to the different growth rates of planes. The rapidly growing plane disappears quickly in the hydrothermal process retaining the slowest growing planes in a larger area. This habit of growth leads to the pencil-like tip at the (0001) plane of c-axis. The plane $(000\bar{1})$ which is the slowest growing plane in ZnO remains in the larger area than the other planes. The growth on the single layer thickness has produced sparsely populated bunches consisting of pencil-tip like nanorods. The emergence of tip with a lesser diameter than that of the base rod may be due to the limited availability of the growth components in the solution. Since the (0001) plane is the fastest growing plane, even before the radial growth finishes completely, the axial growth dominates and, therefore, pencil tips with lesser diameters are formed. Since the nonpolar planes on the side faces of hexagonal pyramids are more stable than the axial plane [22], they could not have dissolved to give this reduction in the diameter of the rods.

The mineralisers NaOH, or NH_3 whichever is used in appropriate cases, give rise to the formation of intermediate complexes as shown by the equations hereunder.

$$NH_3 + H_2O \rightarrow NH_4^+ + OH^- \quad (1)$$

$$Zn^{2+} + 4OH^- \rightarrow Zn(OH)_4^{2-} \quad (2)$$

$$Zn^{2+} + 4NH_3 \rightarrow Zn(NH_3)_4^{2+} \quad (3)$$

From these two intermediate complexes, ZnO is formed as illustrated in the following equations:

$$Zn(OH)_4^{2-} \rightarrow ZnO + H_2O + 2OH^- \quad (4)$$

$$Zn(NH_3)_4^{2+} + 2OH^- \rightarrow ZnO + 4NH_3 + H_2O \quad (5)$$

The reaction of hexamethylene tetramine for the formation of ZnO can be given by the following reaction sequence:

$$(CH_2)_6N_4 + 6H_2O \rightarrow 4NH_3 + 6HCHO \quad (6)$$

$$NH_3 + H_2O \rightarrow NH_4^+ + OH^- \quad (7)$$

$$Zn^{2+} + 2OH^- \rightarrow ZnO + H_2O \quad (8)$$

When zinc nitrate and hexamine are the constituents of the mother liquor, the resultant morphology obtained was nearly a hexagonal diskette shaped one. These structures with a suppressed axial growth are produced only when hexamine was used as the anion generating agent. The anion producing capability of hexamine is very slow and lesser when compared to the effective and quicker OH^- generating property of ammonia-water. The growth units $Zn(OH)_4^{2-}$ are necessary in large number for the growth to progress. In addition to OH^- ions, ammonia water also produces $[Zn(NH_3)_4^{2+}]$ zinc-ammonia complex which can also contribute to the growth in the higher pH conditions [23–25]. The absence of $[Zn(NH_3)_4^{2+}]$ complexes in a hexamine solution is the reason for the suppressed axial growth. In the other case, when zinc acetate dihydrate is used in addition to $ZnNO_3$, a poorly defined popcorn-like shapes with concave finished ends are observed. Here, the excess Zn^{2+} ions are available since sulphate and acetate salts both are used. So, they may result in a faster growth, and after a particular point of time, the solution will try to maintain the equilibrium which should contain a minimum population of Zn cations. So, the grown structure could have followed a reversal process of dissolution. The concanve features may be an indication of the evolution of the dissolution.

8 Atomic force microscopy analysis

In the surface topography analysis taken for the closest packed structure (ZnO-E), they exhibit a uniform sized and spaced granular growth. In Fig. 6(a), the scale depicts a maximum height of 903 nm, while most of the area is covered up to a growth of nearly half of the maximum height (≈450 nm). A profile was taken along the diagonal of the image as shown by the line segment in Fig. 6(b), by using the WSXM software. It has shown a uniformly sized hillocks of nearly half of the maximum (325 nm) within the area of 3.5 μm × 323 nm, which is an indication of a good uniform growth along the shown area. Figure 6(d) shows the 3D picture of the same 2D area.

9 Conclusion

Preparation of a variety of shapes of ZnO nanostructures like vertical hexagonal nanorods, skewed hexagonal

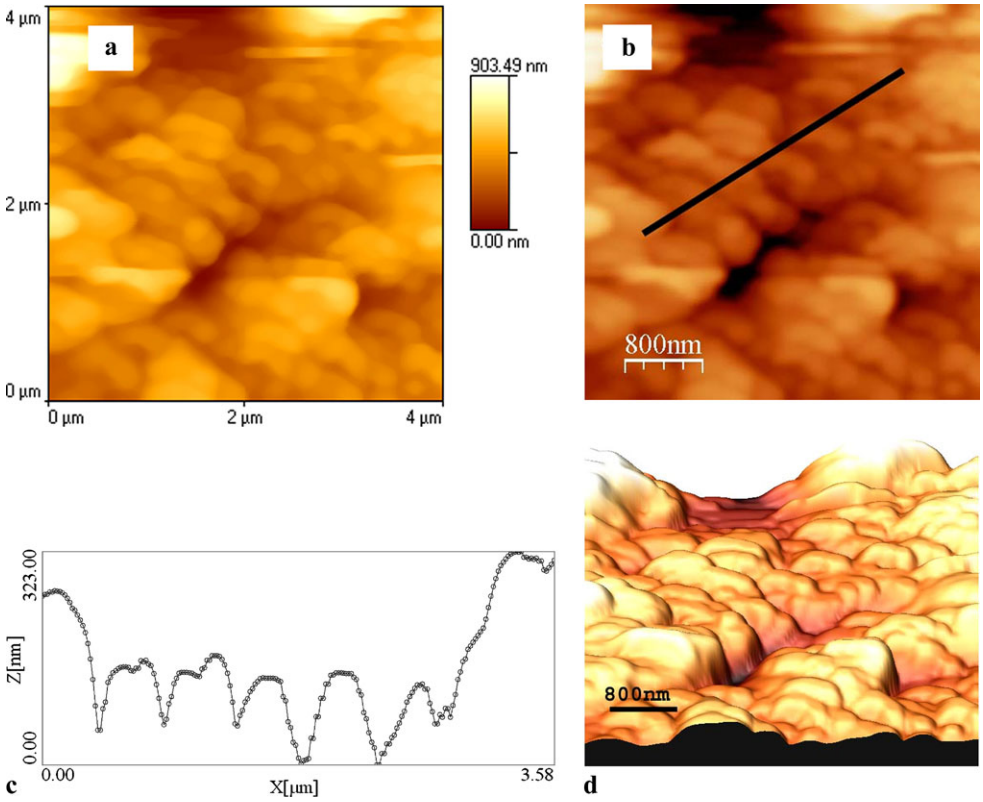

Fig. 6 Surface topography analysis of closest packed nanostructure (ZnO-E) by Atomic Force Microscopy: (**a**) 2D image, (**b**) same 2D image showing the line along which the line profile is taken, (**c**) the profile showing uniform hillocks, (**d**) the simulated 3D-image of the same area as in the 2D image

nanorods, multi-angular peculiar pencil-tipped nanorods bunches, uniformly sized and shaped nanotwigs, closest packed nanofibres array, hexagonal diskette-like nanostructure, and popcorn-like nanostructure with cavities are obtained by simply altering the chemical composition, the seed layer thickness, strength of the cationic source, and a combination of choice of anion generating agents. The texture co-efficient, aspect ratio, morphology of the structures, and a improved surface profile were successfully evidenced to get altered by tuning the chosen experimental parameters. The variation in growth kinetics for the formation of modified structures has been vividly discussed for parallel orientation perpendicular and multi-angular orientation on the basis of activation energy barrier for the formation of heterogeneous nucleations. The route of formation of ZnO through intermediate complexes is proclaimed by the way of simple chemical equations. The aqueous chemical growth of ZnO nanostructures has been utilised and successfully demonstrated as a versatile method for the fabrication of tailor-made morphologies, by influencing the growth kinetics by simply modifying the experimental growth parameters.

Acknowledgements The authors sincerely wish to acknowledge the support from Professor P. Manisankar, Professor and Head, School of Chemistry, Alagappa University for AFM images. The support from Raman Ravikumar and K. Kumar for XPS analysis is gratefully remembered.

References

1. J.H. Kim, D. Andeen, F.F. Lange, Adv.Mater. **18**, 2453–2457 (2006)
2. Q. Ahsanulhaq, A. Umar, Y.B. Hahn, Nanotechnol. **18**, 115603 (2007)
3. C. Jiang, W. Zhang, G. Zou, W. Yu, Q. Yitai, J. Phys. Chem. B. **109**(4), 1361 (2005)
4. D. Ito, M.L. Jespersen, J.E. Hutchison, ACSNano **2**(10), 2001–2006 (2008)
5. J. Song, S. Lim, J. Phys. Chem. C **111**, 596 (2007)
6. J. Ge, B. Tang, L. Zhuo, Z. Shi, Nanotechnol. **17**, 171316 (2006)
7. H.T. Ng, J. Han, T. Yamada, P. Nguyen, Y.P. Chen, M. Meyyappan, Nano Lett. **4**, 1247–1252 (2004)
8. M.S. Arnold, P. Avouris, Z.W. Pan, Z.L. Wang, J. Phys.Chem. B **107**, 659–663 (2003)
9. J.C. Johnson, K.P. Knutsen, H.Q. Yan, M. Law, Y.F. Zhang, P.D. Yang, R.J. Saykally, Nano Lett. **4**, 197–204 (2004)
10. P. Hari, D. Spencer, Phys.Status Solidi C **6**(S1), S150–S153 (2009)
11. S. Ashoka, G. Nagaraju, C.N. Tharamani, G.T. Chandrappa, Mater Lett. **36**, 873–876 (2009)
12. X.M. Sun, X. Chen, Z.X. Deng, Y.D. Li, Mat. Chem Phys. **78**, 99–104 (2002)
13. Y. Lee, Y. Zhang, S.L.G. Ng, F.C. Kartwidjaja, J. Wang, J. Am. Ceram. Soc. **92**(9), 1940–1945 (2009)
14. P. Mitra, J. Khan, Mat. Chem. Phys. **98**, 279–284 (2006)
15. X.D. Gao, X.M. Li, W.D. Yu, J. Solid State. Chem **177**, 3830–3834 (2004)
16. L. Vayssieres, Int. J. of Nanotechnology **1**, 1 (2004)
17. T. Mahalingam, K.M. Lee, S. Lee, Y. Ahn, J.-Y. Park, K.H. Koh, K.H. Park, Nanotechnology **17**, 1–5 (2006)
18. W. Peng, X. Qu, G. Cong, Z. Wang, Cryst. Growth. Des. **6**, 1548 (2006)

19. H. Zhang, D. Yang, Y. Ji, X. Ma, J. Xu, D. Que, J. Phys. Chem. B **108**, 1355 (2004)
20. Y. Tak, K. Yong, J.Phys. Chem. B **109**, 19263–19269 (2005)
21. M. Wang, E.J. Kim, E.W. Shin, J.S. Chung, S.H. Hahn, C. Park, J.Phys.Chem. C **112**, 1920–1924 (2008)
22. L. Vayssieres, K. Keis, A. Hagfeldt, S.E. Lindquist, Chem. Mater. **15**, 622 (2001)
23. J. Zhang, L. Sun, J. Yin, H. Su, C. Liao, C. Yan, Chem.Mater. **14**, 4172 (2002)
24. A. Wei, X.W. Sun, C.X. Xu, Z.L. Dong, Y. Yang, S.T. Tan, W. Huang, Nanotechnology **17**, 1740 (2006)
25. Y. Fang, Q. Pang, X. Wen, J. Wang, S. Yang, Small **2**, 612 (2006)